Data assimilation for terrestrial magnetism

A. Fournier (IPGP) fournier@ipgp.fr

J. Aubert (IPGP), E. Cosme (University of Grenoble), G. Hulot (IPGP), Y. Gallet (IPGP), M. Morzfeld (University of Arizona), Lars Nerger (Alfred Wegener Institute), S. Sanchez (MPS Gottingen), E. Thébault (LPG Nantes)

Institut de Physique du Globe, Paris, France

March 1st, 2017 – Riken International Symposium on Data Assimilation

Outline

1. Introduction: Observations & Motivation
2. Two examples of application

The Earth's interior and the geomagnetic field

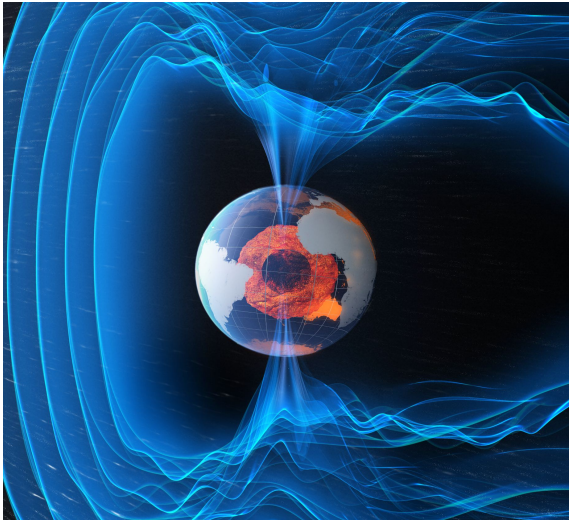

© European Space Agency (www.esa.int/swarm)

The Earth's interior and the geomagnetic field

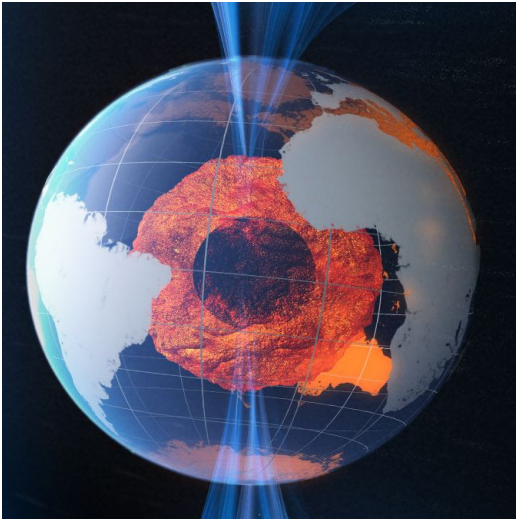

The Earth's interior and the geomagnetic field

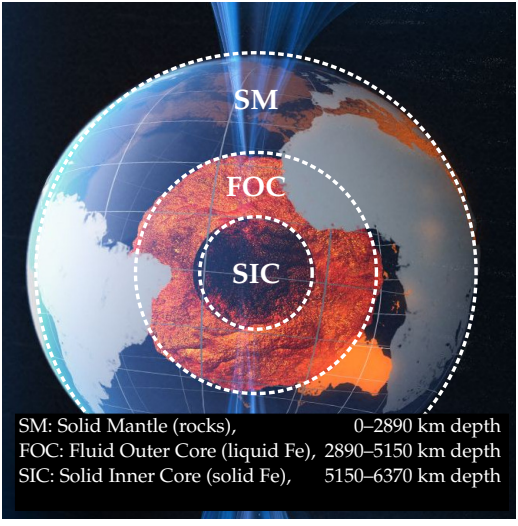

The internal field

Spherical harmonic analysis

$$
\begin{aligned}
\boldsymbol{B} &= -\boldsymbol{\nabla} V \text{ in a current-free region; with internal sources,} \\
V(r,\theta,\varphi,t) &= a \sum_{\ell,m} \left(\frac{a}{r}\right)^{\ell+1} \left[g_\ell^m(t) \cos m\varphi + h_\ell^m(t) \sin m\varphi \right] P_\ell^m(\cos\theta), \\
B_r(r,\theta,\varphi,t) &= \sum_{\ell,m} \left(\frac{a}{r}\right)^{\ell+2} \left[g_\ell^m(t) \cos m\varphi + h_\ell^m(t) \sin m\varphi \right] P_\ell^m(\cos\theta).
\end{aligned}
$$

Connection between surface observations and the field at the CMB

(CMB: Core-Mantle Boundary)

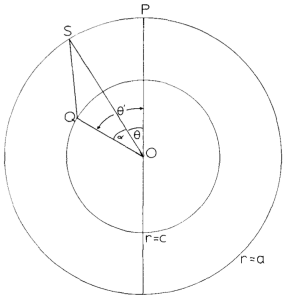

Figure 1. Geometry for the superposition integral (3). O is the origin of a system of spherical polar coordinates with pole P. The site is at S(θ, ϕ) on the surface of the Earth. The Green's function $N(Y, \theta, \phi; \theta', \phi')$, is the potential at S due to a singularity of unit strength in the radial field at point (θ', ϕ') on the core–mantle boundary. N is symmetric about the axis OS and is a function only of α, the angular distance between Q and S. N is a maximum when Q is immediately beneath S, and decreases monotonically with increasing angular and distance α.

Gubbins and Roberts (1983)

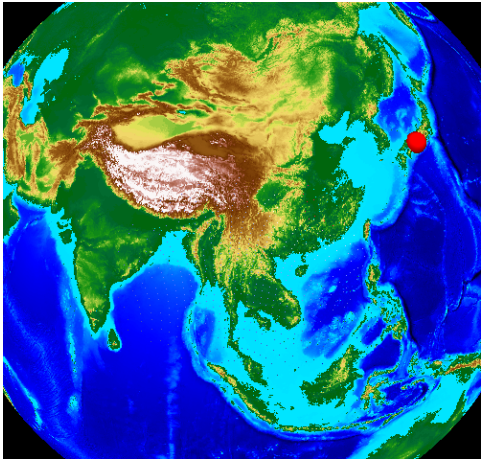

Connection between surface observations and the field at the CMB

(CMB: Core-Mantle Boundary)

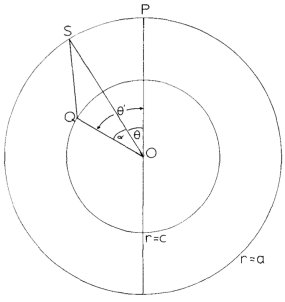

Figure 1. Geometry for the superposition integral (3). O is the origin of a system of spherical polar coordinates with pole P. The site is at S(θ, ϕ) on the surface of the Earth. The Green's function $N(Y, \theta, \phi; \theta', \phi')$, is the potential at S due to a singularity of unit strength in the radial field at point (θ', ϕ') on the core–mantle boundary. N is symmetric about the axis OS and is a function only of α, the angular distance between Q and S. N is a maximum when Q is immediately beneath S, and decreases monotonically with increasing angular and distance α.

Gubbins and Roberts (1983)

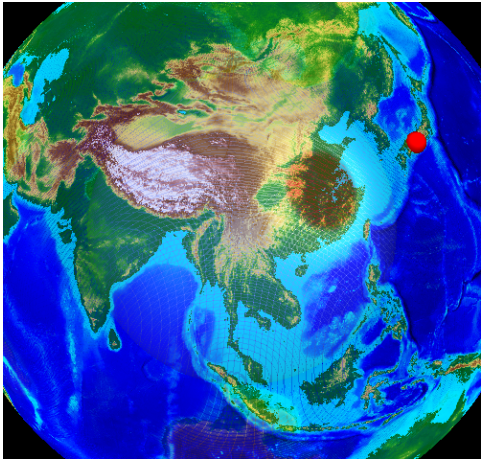

Connection between surface observations and the field at the CMB

(CMB: Core-Mantle Boundary)

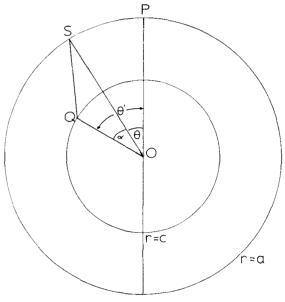

Figure 1. Geometry for the superposition integral (3). O is the origin of a system of spherical polar coordinates with pole P. The site is at S(θ, ϕ) on the surface of the Earth. The Green's function $N(Y, \theta, \phi; \theta', \phi')$, is the potential at S due to a singularity of unit strength in the radial field at point (θ', ϕ') on the core–mantle boundary. N is symmetric about the axis OS and is a function only of α, the angular distance between Q and S. N is a maximum when Q is immediately beneath S, and decreases monotonically with increasing angular and distance α.

Gubbins and Roberts (1983)

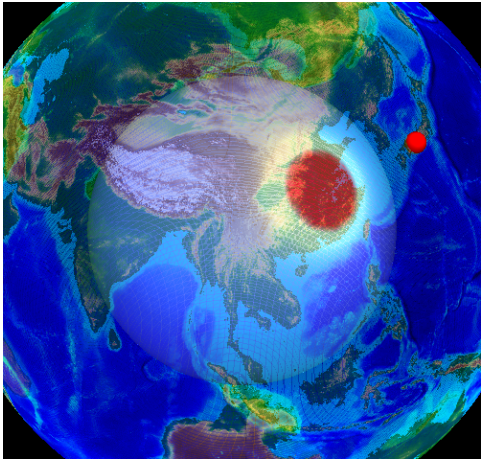

Connection between surface observations and the field at the CMB

(CMB: Core-Mantle Boundary)

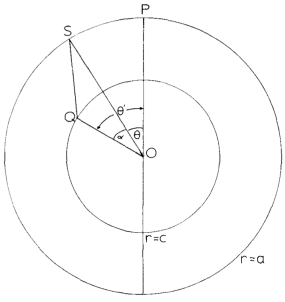

Figure 1. Geometry for the superposition integral (3). O is the origin of a system of spherical polar coordinates with pole P. The site is at S(θ, ϕ) on the surface of the Earth. The Green's function $N(Y, \theta, \phi; \theta', \phi')$, is the potential at S due to a singularity of unit strength in the radial field at point (θ', ϕ') on the core–mantle boundary. N is symmetric about the axis OS and is a function only of α, the angular distance between Q and S. N is a maximum when Q is immediately beneath S, and decreases monotonically with increasing angular and distance α.

Gubbins and Roberts (1983)

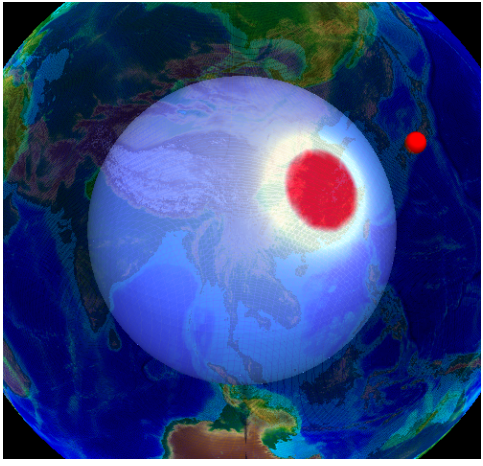

Connection between surface observations and the field at the CMB

(CMB: Core-Mantle Boundary)

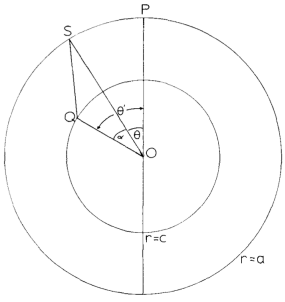

Figure 1. Geometry for the superposition integral (3). O is the origin of a system of spherical polar coordinates with pole P. The site is at S(θ, ϕ) on the surface of the Earth. The Green's function $N(Y, \theta, \phi; \theta', \phi')$, is the potential at S due to a singularity of unit strength in the radial field at point (θ', ϕ') on the core–mantle boundary. N is symmetric about the axis OS and is a function only of α, the angular distance between Q and S. N is a maximum when Q is immediately beneath S, and decreases monotonically with increasing angular and distance α.

Gubbins and Roberts (1983)

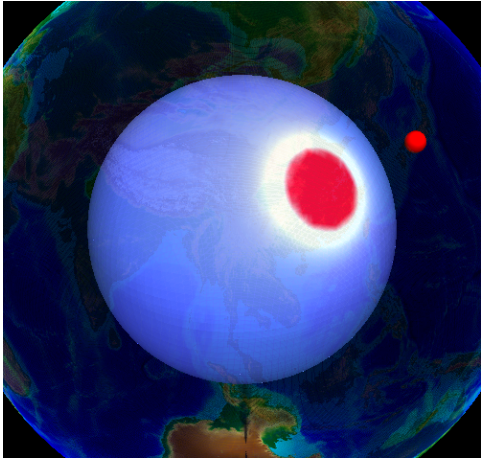

The lithosphere is magnetized

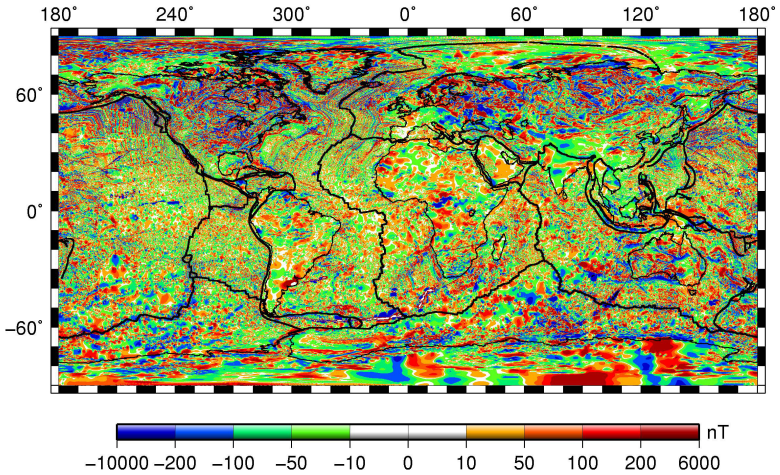

World Digital Magnetic Anomaly Map consortium

The geomagnetic field

To take home

- dipole-dominated
- small scales of dynamo field concealed by the small scales of the crustal field
- even if perfect sampling: $\ell \lesssim 13$ (lateral resolution of $\sim$ 1500 km at the core surface)

The catalogs of data

$\tau_{\text{conv}} \sim 150$ yr $\quad \tau_{\text{diff}} \sim 60,000$ yr

- Paleo-,archeomagnetism: $0 - 10(100, 1000+)$ kyr ago — D, I, F
- Mariners: $0 - 400$ yr ago — D, I
- Observatories: $0 - 150$ yr ago — X, Y, Z
- Satellites: $0 - 20$ yr ago — X, Y, Z

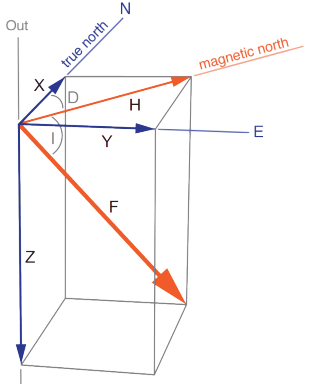

A heterogeneous record: spatial coverage (courtesy Chris Finlay)

archeo/paleo: 0 – 10+ **kyr ago**

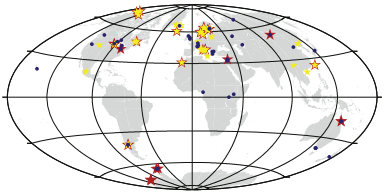

Locations of lake sediment records used to constrain the CALS10k model of **Korte et al. (EPSL, 2011)** spanning the past 10kyrs.

logbooks: 0 – 400 **yr ago**

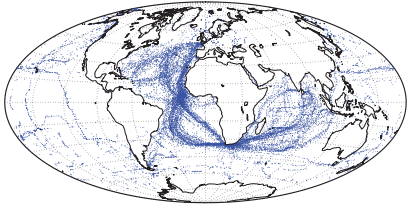

Locations of historical data (all components) between 1770 and 1790 from the **Jonkers et al. (Rev. Geophys., 2003)** database.

observatories: 0 – 150 **yr ago**

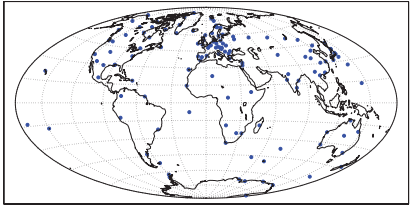

Locations of observatories used in determination of recent internal field models.

satellites: 0 – 20 **yr ago**

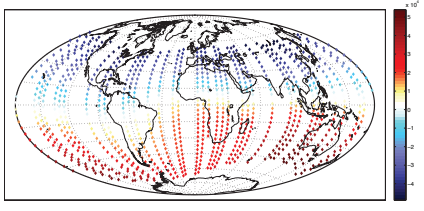

Example showing 3 days of CHAMP vector satellite data from 2009

Synthesis

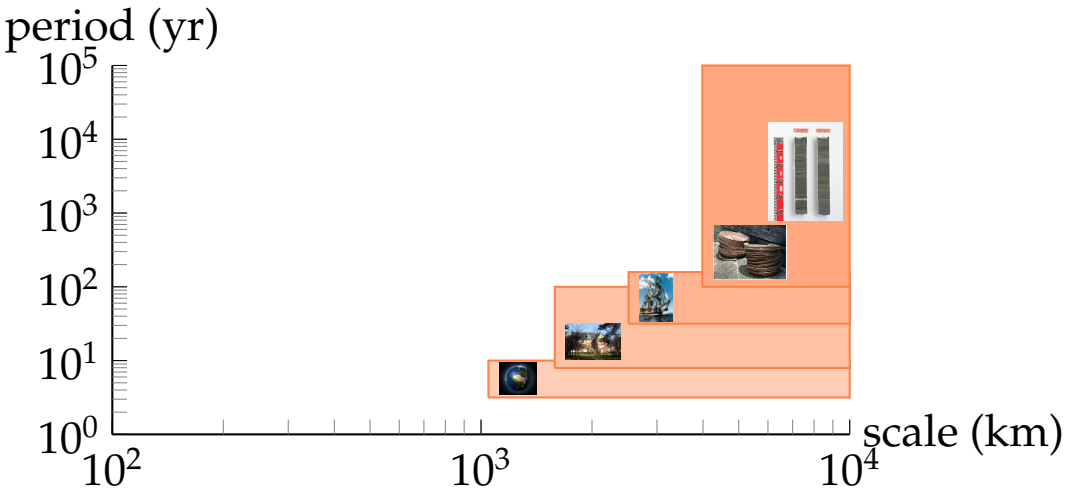

Synthesis

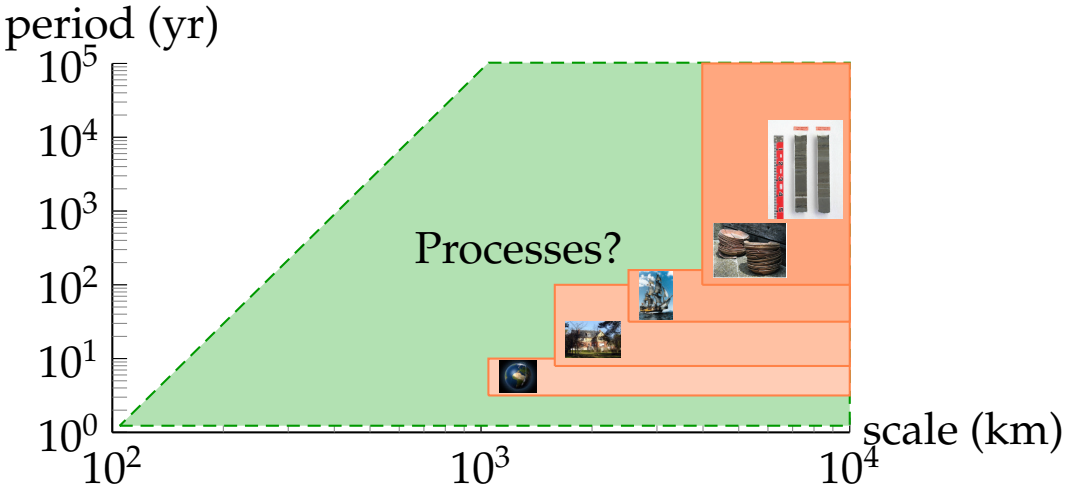
period (yr)
10^5
10^4
10^3
10^2
10^1
10^0
Processes?
10^2
10^3
10^4
scale (km)

Data assimilation in geomagnetism

Principle

To analyse the variations of the geomagnetic field reflected in the highly heterogeneous record at our disposal using a dynamical model of its evolution as source of prior information

Ingredients

- observations
- physical laws (dynamical model)

Goals

- Identify those physical processes controlling the geomagnetic secular variation
  important because fundamental
- Estimate the internal magnetohydrodynamic structure of Earth's core
- Forecast the evolution of the geomagnetic field
- Reanalyze its past variations

Data assimilation in geomagnetism

Principle

To analyse the variations of the geomagnetic field reflected in the highly heterogeneous record at our disposal using a dynamical model of its evolution as source of prior information

Ingredients

- observations
- physical laws (dynamical model)

Goals

- Identify those physical processes controlling the geomagnetic secular variation
  important because fundamental
- Estimate the internal magnetohydrodynamic structure of Earth's core
- Forecast the evolution of the geomagnetic field
- Reanalyze its past variations

2 applications (research stage)

1. Assimilation of archeomagnetic data into a 3D numerical model of the geodynamo (3 ka)
2. Assimilation of dipole intensity data spanning the past 2 Ma into a low-dimensional model of geomagnetic reversals

1. Assimilation of archeomagnetic data into a 3D numerical model of the geodynamo (3 ka)

Sabrina Sanchez' PhD (2016)

Convection-driven models of the geodynamo

A dynamo is a system which has the ability to convert mechanical energy into electromagnetic energy. **In Earth's core, it is the convective flow u of liquid iron which sustains the magnetic field B against Ohmic decay**.

A model of the geodynamo in a nutshell

- Conservation laws (mass, momentum, energy) and Maxwell's equations (MHD approximation)
- Set of 3D non-linear coupled PDEs to solve in a spherical shell (the FOC)
- Pseudo-spectral method (Glatzmaier, 1984): finite difference in radius, spherical harmonics in the horizontal plane (Dormy, 1997).
- Size of state vector $\sim 10^6 - 10^7$.

The ensemble Kalman filter: Implementation

- The starting dynamo code:
  a modified (more modular) version of the in-house PARODY code (Dormy et al., 1998; Aubert et al., 2008).
  + SHTns library (Schaeffer, 2013).
- The EnKF layer:
  a suitably modified version of the Parallel Data Assimilation Framework of Nerger and Hiller (2013).


Contents lists available at SciVerse ScienceDirect

Computers & Geosciences

journal homepage: www.elsevier.com/locate/cageo

Software for ensemble-based data assimilation systems—Implementation strategies and scalability

Lars Nerger*, Wolfgang Hiller

Alfred Wegener Institute for Polar and Marine Research, Am Handelshafen 12, D-27570 Bremerhaven, Germany

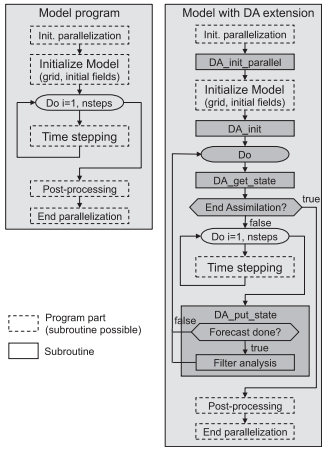

Fig. 1. Left: Flow diagram of a typical numerical model. Right: Flow diagram of the model extended to an assimilation system by calls to routines of the assimilation framework. (Based on Nerger et al., 2005b.)

Nerger and Hiller (2013); http://pdaf.awi.de

(almost) Embarassingly parallel setup: Efficiency > 99 % on 1,440 cores (Fournier et al., 2013)

The archeomagnetic data

Distribution in time

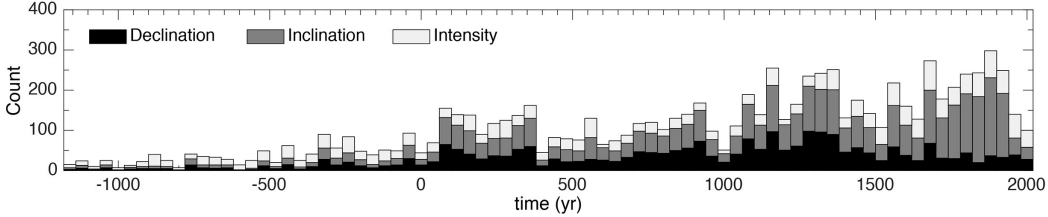

First assimilation experiments using these pointwise measurements

- one analysis every 20 yr (numerical time step $\sim$ 2 days)
- ensemble size: 512

Initial finding with real data

- The database contains data whose locations are close but whose values are moderately compatible with each other
- Strong gradients of B_r at the core-mantle boundary: unstable scheme

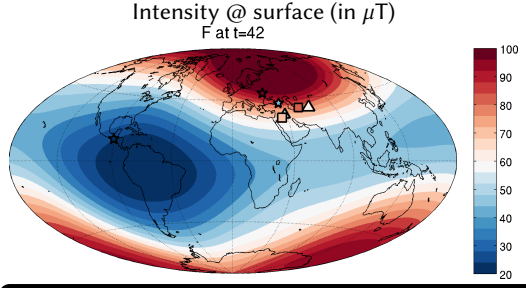

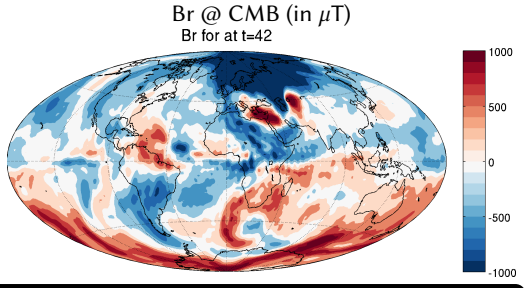

Empirical fix (in spectral space) : $\mathbf{P}^f \rightarrow \tilde{\mathbf{P}}^f$

Each component of degree ℓ of each $\mathbf{x}^f$ is scaled by $\rho(\ell)$ with

$$\begin{aligned} \rho(\ell) &= 1 \text{ for } \ell \leq 5, \\ \rho(\ell) &\propto \ell^{-2} \text{ for } \ell > 5. \end{aligned}$$

Variance of the ensemble

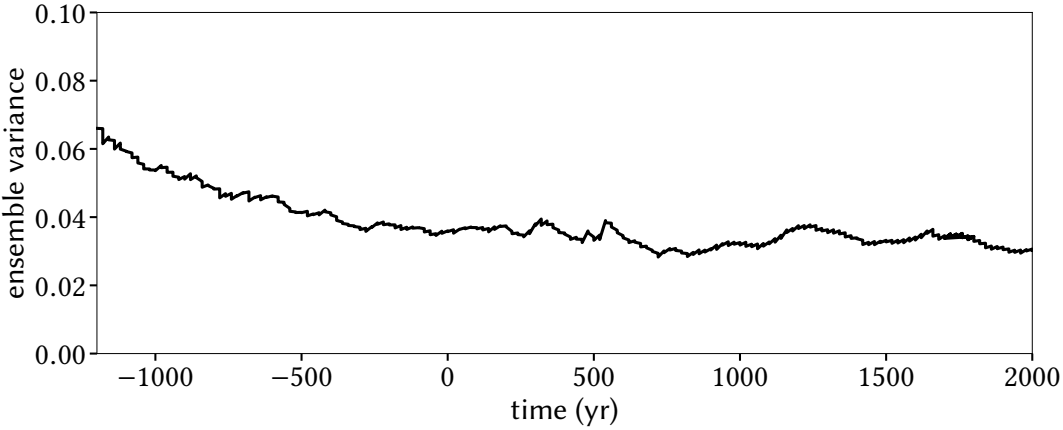

Axial dipole - g_1^0

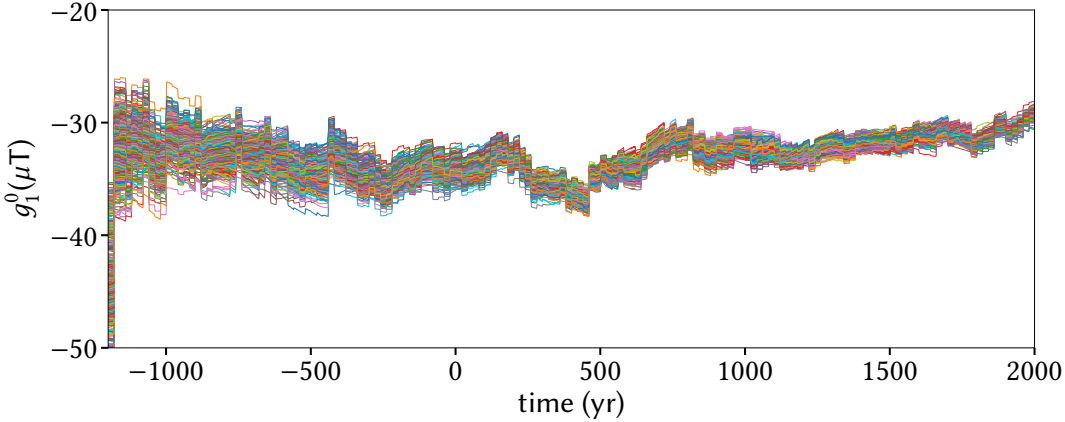

2. Assimilation of dipole intensity data spanning the past 2 Ma into a low-dimensional model of geomagnetic reversals

Coarse predictions of dipole reversals (Morzfeld et al., PEPI, 2017)

Paleomagnetic data

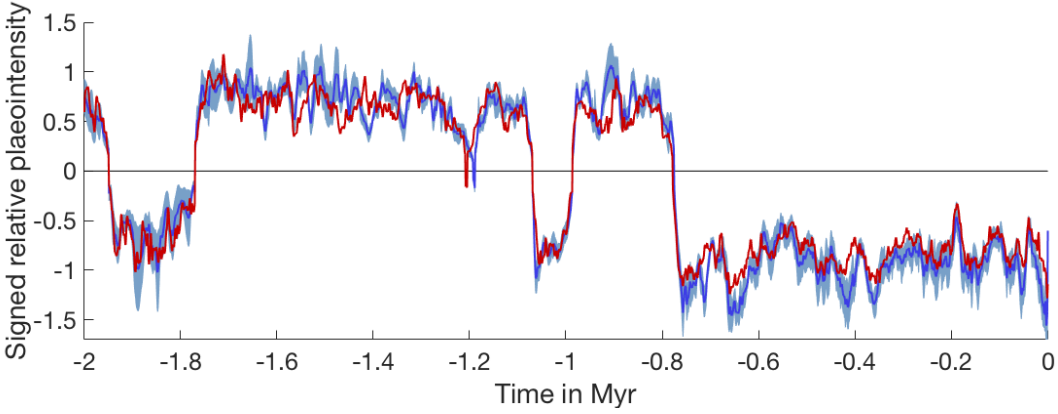

Signed relative paleointensity. The blue line represents the signed Sint-2000 data (Valet et al., 2005) and the light blue cloud represents a 95% confidence interval. The red line represents the mean of the PADM2M data (Ziegler et al., 2011). **One datum every 1,000 years.**

A low-dimensional deterministic model of dipole reversals

Gissinger (2012)

$$\begin{aligned} \frac{dQ}{dt} &= \mu Q - VD, \\ \frac{dD}{dt} &= -\nu D + VQ, \\ \frac{dV}{dt} &= \Gamma - V + QD, \end{aligned}$$

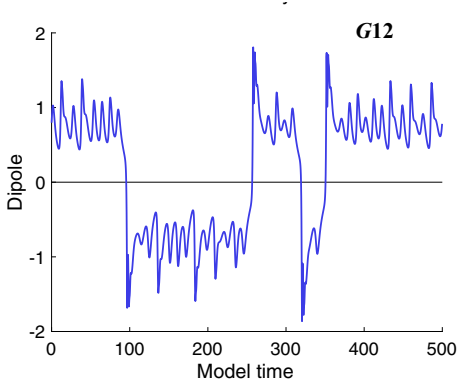

Morzfeld et al. (2017)

Data assimilation

We considered the EnKF (Evensen, 2006) and implicit sampling (Chorin and Tu, 2009; Chorin et al., 2010; Morzfeld et al., 2012; Atkins et al., 2013; Morzfeld and Chorin, 2012).

Relative error

$$e = \frac{\sum_{n=1}^{2000} \left(z^n - \hat{E}\left[x^n | z^{1:n}\right] \right)^2}{\sum_{n=1}^{2000} (z^n)^2},$$

where z^n are the data at time n kyr and $\hat{E}\left[x^n | z^{1:n}\right]$ is the approximation of the conditional mean of the dipole given the data up to time n kyr.

		G12				
	Method:	EnKF	IMP			
	Data/sweep:	1	1	5	10	15
	# samples					
Sint-2000	50	30.5	5.70	3.74	4.28	10.90
	100	30.7	5.43	3.80	4.20	10.93
	200	30.0	5.38	3.61	6.19	10.91
	400	29.5	5.39	3.51	6.18	10.88
PADM2M	50	27.1	6.63	5.09	5.98	10.7
	100	27.9	6.27	4.92	5.93	10.5
	200	26.5	5.99	4.99	5.93	10.9
	400	26.8	5.83	4.92	5.83	10.7

Hincasting the last reversal

The Brunhes-Matuyama reversal occurs between 777 and 776 kyr ago.

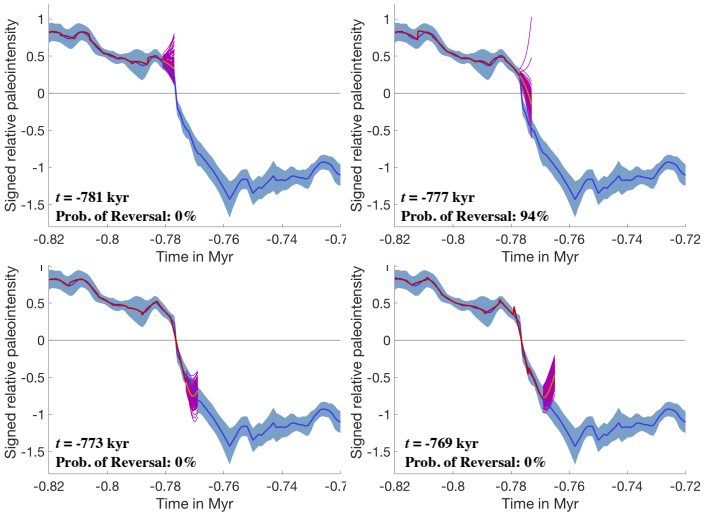

Prediction: is a reversal going to happen within the next 4 kyr?

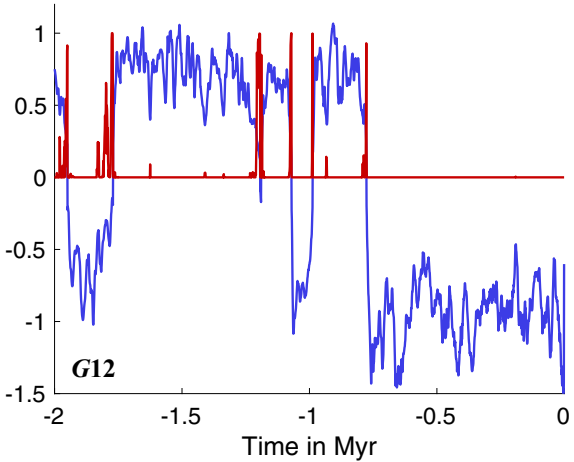

Shown is the predicted probability of a reversal to occur within 4 kyr as function of time (red) along with the Sint-2000 data (blue).

Summary: some aspects of DA in geomagnetism

EnKF applied to a full dynamo model

- Assimilation of pointwise archeomagnetic observations spanning the past 3,000 years
- Empirical fix to cope with the heterogeneity within the dataset
- Systematic study (ensemble size, data selection, etc.)
- Combine archeomagnetic, historical and satellite data (EnKS)
- Prediction (under uncertainty) of the evolution of structure of the field

Low-dimensional modelling of geomagnetic reversals

- No reversal in sight!
- Improve low-dimensional model
- Good news: longer paleointensity records are being built (2 Ma $\rightarrow$ 5 Ma)

References I

Atkins, E., M. Morzfeld, and A. Chorin (2013). Implicit particle methods and their connection with variational data assimilation. *Monthly Weather Review 141*, 1786–1803.

Aubert, J., J. Aurnou, and J. Wicht (2008). The magnetic structure of convection-driven numerical dynamos. *Geophysical Journal International 172*(3), 945–956.

Chorin, A., M. Morzfeld, and X. Tu (2010). Implicit particle filters for data assimilation. *Communications in Applied Mathematics and Computational Science 5*(2), 221–240.

Chorin, A. and X. Tu (2009). Implicit sampling for particle filters. *Proceedings of the National Academy of Sciences 106*(41), 17249–17254.

Dormy, E. (1997). *Modélisation numérique de la dynamo terrestre*. Ph. D. thesis, Institut de Physique du Globe de Paris.

Dormy, E., P. Cardin, and D. Jault (1998). MHD flow in a slightly differentially rotating spherical shell, with conducting inner core, in a dipolar magnetic field. *Earth and Planetary Science Letters 160*(1-2), 15–30.

Evensen, G. (2006). *Data assimilation: the ensemble Kalman filter*. Springer.

Fournier, A., L. Nerger, and J. Aubert (2013). An ensemble Kalman filter for the time-dependent analysis of the geomagnetic field. *Geochemistry, Geophysics, Geosystems 14*, 4035–4043. doi:10.1002/ggge.20252.

Glatzmaier, G. A. (1984). Numerical simulations of stellar convective dynamos. I- The model and method. *Journal of Computational Physics 55*(3), 461–484.

Gubbins, D. and N. Roberts (1983). Use of the frozen flux approximation in the interpretation of archaeomagnetic and palaeomagnetic data. *Geophysical Journal of the Royal Astronomical Society 73*(3), 675–687.

References II

Morzfeld, M. and A. Chorin (2012). Implicit particle filtering for models with partial noise, and an application to geomagnetic data assimilation. *Nonlinear Processes in Geophysics 19*, 365–382.

Morzfeld, M., A. Fournier, and G. Hulot (2017). Coarse predictions of dipole reversals by low-dimensional modelling and data assimilation. *Physics of the Earth and Planetary Interiors 262*, 8–17.

Morzfeld, M., X. Tu, E. Atkins, and A. Chorin (2012). A random map implementation of implicit filters. *Journal of Computational Physics 231*, 2049–2066.

Nerger, L. and W. Hiller (2013). Software for ensemble-based data assimilation systems—Implementation strategies and scalability. *Computers & Geosciences 55*, 110–118.

Sanchez, S. (2016). *Assimilation of geomagnetic data into dynamo models, an archeomagnetic study*. Ph. D. thesis, Institut de Physique du Globe de Paris.

Schaeffer, N. (2013). Efficient spherical harmonic transforms aimed at pseudospectral numerical simulations. *Geochemistry, Geophysics, Geosystems 14*(3), 751–758.

Valet, J.-P., L. Meynadier, and Y. Guyodo (2005). Geomagnetic field strength and reversal rate over the past 2 million years. *Nature 435*, 802–805.

Ziegler, L. B., C. G. Constable, C. L. Johnson, and L. Tauxe (2011). PADM2M: a penalized maximum likelihood model of the 0-2 Ma paleomagnetic axial dipole model. *Geophysical Journal International 184*(3), 1069–1089.

Threshold-based predictions

- Intensity based - if the intensity drops below F_{min}, the field will reverse (**no physics**)
- Probability based - if the DA based probability exceeds p_{crit}, the field will reverse (**low-d physics**)

F_{min} and p_{crit} are determined based on the first Myr (training set) and then tested over the second Myr (verification data).

Threshold-based predictions

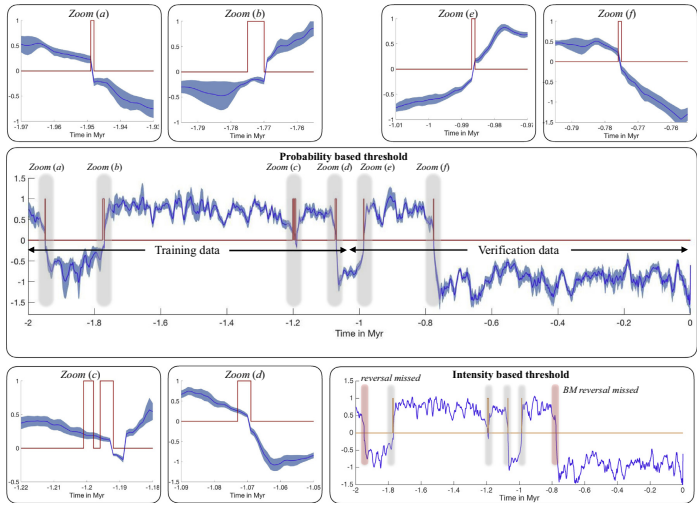

Morzfeld et al. (2017)

The Earth's main magnetic field

B_r (nT) at Earth's surface in 2007

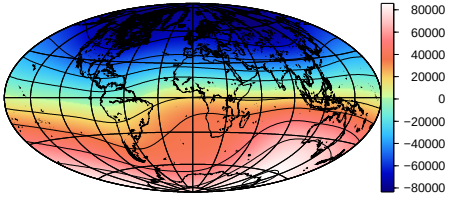

B_r (nT) at the core surface in 2007

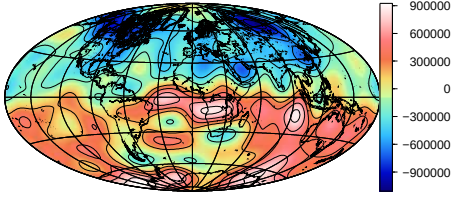

Mauersberger–Lowes spectrum

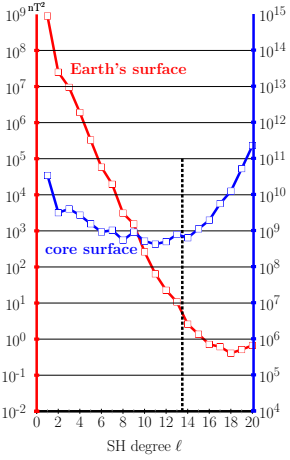

CHAOS2 model (1997-2009), Olsen et al., GJI, 2009

Estimate (ensemble mean) since 1700

Scale for radial field: ± 1 mT. Scale for azimuthal flow: ± 30 km/yr

Axial dipole - g_1^0

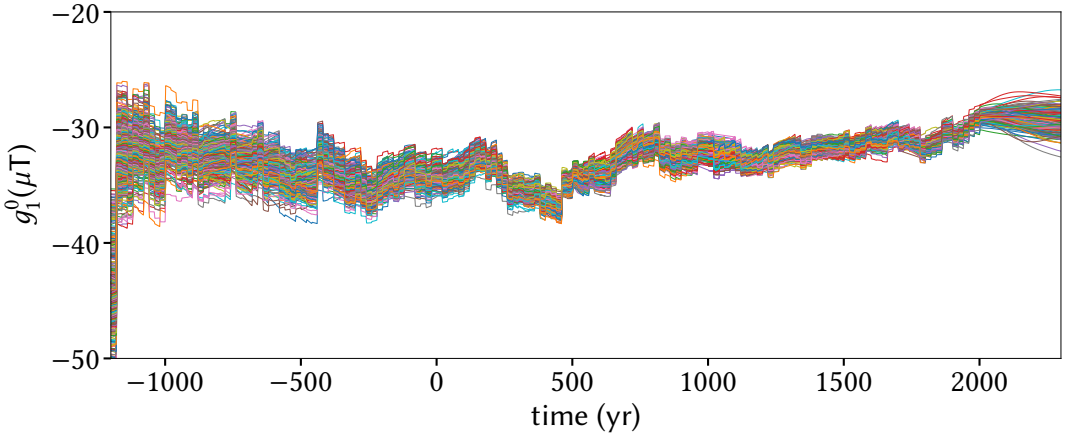

Measurements and sources of the geomagnetic field

The geodynamo accounts for more than 90% of the field measured at the Earth's surface.

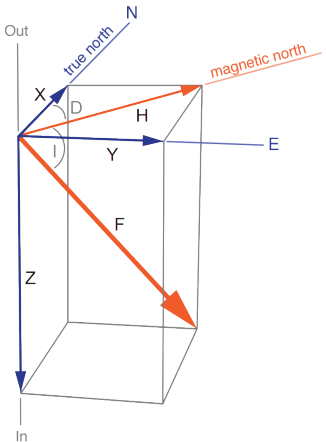

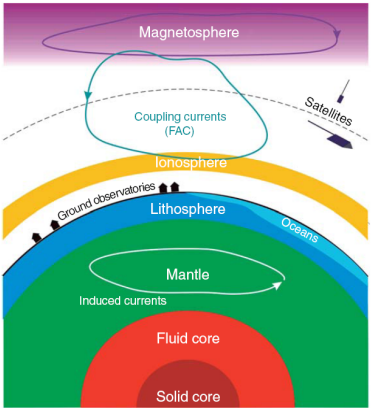

Figure 1 Sketch of the various sources contributing to the near-Earth magnetic field.

Hulot et al. (Treatise on Geophysics, 2nd ed., 2015)